Nuclear Engineering and Technology 52 (2020) 2717–2724

Contents lists available at ScienceDirect

Nuclear Engineering and Technology

journal homepage: www.elsevier.com/locate/net

Original Article

Comprehensive validation of silicon cross sections

Tomáš Czakoj [a, *], Michal Košťál [a], Jan Šimon [a], Jaroslav Šoltés [a], Martin Mareček [a], Roberto Capote [b]

[a] Research Centre Rez Ltd, 250 68, Husinec-Řež 130, Czech Republic
[b] NAPC—Nuclear Data Section, International Atomic Energy Agency, A-1400, Vienna, Austria

ARTICLE INFO

Article history:
Received 19 December 2019
Received in revised form
8 April 2020
Accepted 18 May 2020
Available online 26 May 2020

Keywords:
INDEN evaluation of Si cross section
LR-0
Critical experiment
Spectrum measurement
SiO2 thermal scattering law

ABSTRACT

Silicon, especially silicon in the form of SiO_2, is a major component of rocks. Final spent fuel storages, which are being designed, are located in suitable rock formations in the Earth's crust. Reduction of the uncertainty of silicon neutron scattering and capture is needed; improved silicon evaluations have been recently produced by the ORNL/IAEA collaboration within the INDEN project. This paper deals with the nuclear data validation of that evaluation performed at the LR-0 reactor by means of critical experiments and measurement of reaction rates. Large amounts of silicon were used both as pure crystalline silicon and SiO_2 sand. The critical moderator level was measured for various core configurations. Reaction rates were determined in the largest core configuration. Simulations of the experimental setup were performed using the MCNP6.2 code. The obtained results show the improvement in silicon cross-sections in the INDEN evaluations compared to existing evaluations in major libraries. The new Thermal Scattering Law for SiO_2 published in ENDF/B-VIII.0 additionally reduces the discrepancy between calculation and experiments. However, an unphysical peak is visible in the neutron spectrum in SiO_2 obtained by calculation with the new Thermal Scattering Law.

1. Introduction

Silicon, being more than 25% of the Earth's crust weight [1], is an important part of the Earth. Moreover, silicon is also a fundamental component of concrete, which is an important structural material of all nuclear facilities. Therefore, silicon is very important from the point of view of operational safety, shielding, and criticality safety of long-term storage of nuclear waste.

Due to these reasons, it is necessary to know the silicon cross-sections precisely. Recently, a new reevaluation of silicon cross sections in the resonance region was produced by a collaboration of Oak Ridge National Laboratory and the IAEA within the INDEN project [2]. As a result of this reevaluation, the thermal capture cross-section was increased by 10% and direct capture effects, which are important for the near magic silicon isotopes were properly taken into account. This new evaluation is hereinafter referred to as INDEN. This new evaluation was not available for the last release of the ENDF/B-VIII.0 library [3] which included a new Thermal Scattering Law (hereinafter referred to as TSL) matrix for silicon dioxide [3].

With new silicon evaluations available, it is very valuable to perform targeted integral experiments for their validation as integral experiments typically feature a much lower uncertainty than differential ones. There have been several critical experiments using silicon dioxide sand in the past. These experiments were carried out at the Big Physical Stand (BFS) facility in 1999–2000 in Russia, and they are known as BFS-79 (with uranium fuel) or BFS-81 (with plutonium fuel). These experiments were sponsored by the U.S. National Spent Nuclear Fuel Program [4] and they are listed in the International Handbook of Evaluated Criticality Benchmark Safety Experiments—ICSBEP (HEU-MET-MIXED-005 and PU-MET-MIXED-001) [5].

A new series of critical experiments were recently carried out at the LR-0 reactor to confirm the evaluation of silicon cross-sections and to extend the number of integral experiments with silicon. One of these experiments, containing the highest amount of silicon, was complemented by reaction rates measurements. The reaction rates were determined with the aim to describe the shape of a neutron spectrum in a silicon compound. This description is possible if the used dosimeters and corresponding dosimetry reactions cover the whole energy range of interest.

Three experiments were undertaken. The first experiment was carried out with pure crystalline silicon. The crystalline silicon was

* Corresponding author.
E-mail address: tomas.czakoj@cvrez.cz (T. Czakoj).

https://doi.org/10.1016/j.net.2020.05.019

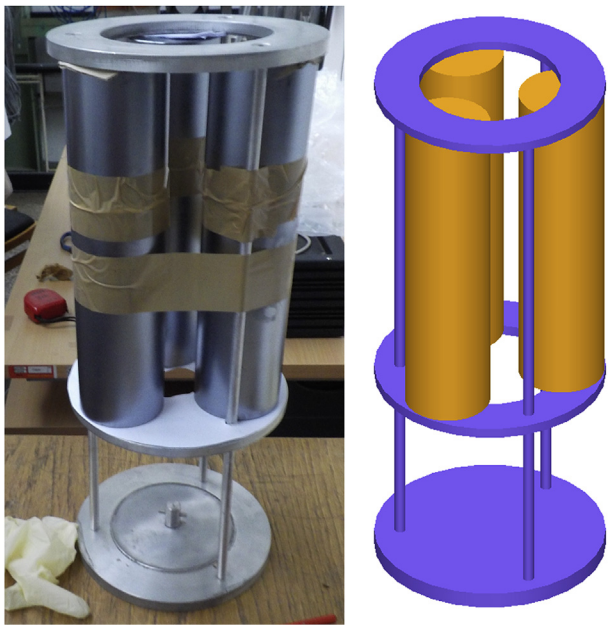

Fig. 1. Photo and visualization of the aluminum holder (violet color) with silicon crystals (orange color). (For interpretation of the references to color in this figure legend, the reader is referred to the Web version of this article.)

used due to its availability at Research Centre Řež (silicon filtered neutron beam at the LVR-15 reactor [6]). The following experiment was performed with silicon dioxide sand, which was used as an inexpensive way to insert a larger amount of silicon into the core. This experiment confirmed the possibility to use sand in the reactor, and a very large amount of sand was used in the last experiment.

2. Methodology of experiments and calculations

The influence of crystalline silicon and silica sand on reactivity has been assessed by comparing the experimentally determined critical configurations and corresponding Monte Carlo calculations. These experiments were carried out at the LR-0 reactor. The LR-0 reactor is zero power light water moderator reactor, and it uses a versatile configuration of VVER-like fuel assemblies. This fuel has almost the same properties as the fuel used in the VVER nuclear power plants. The difference is in the height of fission column, which is reduced to 125 cm. The criticality of the reactor can be controlled by the change of moderator level or by moving the control rods. Cases, when the criticality is controlled by the change of moderator level, have only partially flooded fuel assemblies. Information about critical moderator level adjustment can be found in Ref. [7].

2.1. Experimental setup – criticality

The first experiment, marked as Case 1, was performed with crystalline silicon. Three pieces of silicon crystal (a cylinder with a diameter of 7.8 cm and a height of 30.0 cm, density 2.33 g/cm^3) were fixed in an aluminum holder, and placed into a hexagonal experimental channel (see Fig. 1). This channel was placed into the center of the reactor core, and it was surrounded by six fuel assemblies with a nominal enrichment of 3.3%. This configuration of fuel assemblies is called a benchmark or special core, and it is extensively characterized in Ref. [8]. A schematic drawing of this configuration can be seen in Fig. 2a. Several critical experiments were performed, and the average moderator level is listed in Table 3. Silicon crystals were completely located below the moderator level (see Fig. 3). The experiment was also conducted without insertion of crystalline silicon. This case is then referred to as a void experiment. The void experiment was conducted to set a reference case.

The second experiment, marked as Case 2, was carried out using natural silica sand. Water content in the sand was below 0.0015 wt %, other contaminants were below 10 pcm in terms of reactivity mainly due to the low content of potassium, titanium and iron. Sand with a density of 1.439 g/cm^3 and a total weight of 48.9 kg was poured into a hexagonal aluminum channel. Height of the sand column was 78.2 cm. The channel with sand was placed into the core. The configuration of fuel assemblies was the same as in the previous case (see Figs. 2b and 3). Several critical experiments were performed, and the average moderator level is listed in Table 3. The experiment was also carried out without insertion of sand and is also referred to as a void experiment.

The third experiment, marked as Case 3, was realized using natural silica sand from the same resources as the previous case.

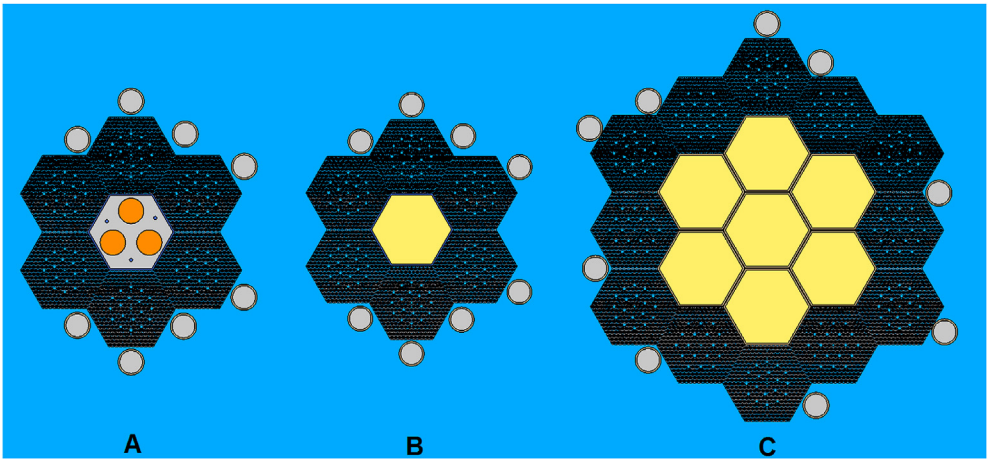

Fig. 2. Core configurations: a) Case 1 - core with crystalline silicon (orange color) b) Case 2 - core with one channel with sand (yellow color) c) Case 3 - core with seven channels with sand (yellow color). (For interpretation of the references to color in this figure legend, the reader is referred to the Web version of this article.)

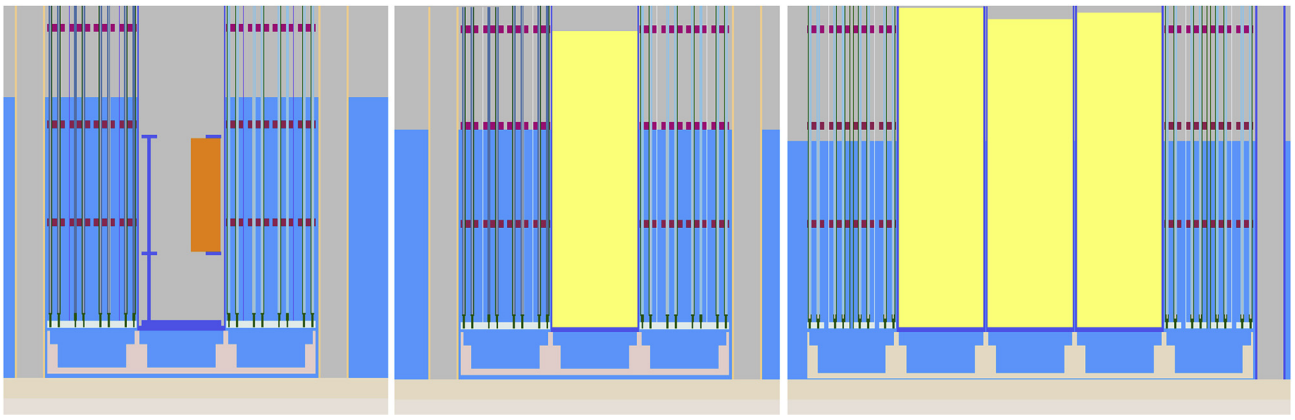

Fig. 3. Schematic drawing of silicon (orange color) and sand (yellow) placed in the experimental channel (Case 1, 2 and 3). (For interpretation of the references to color in this figure legend, the reader is referred to the Web version of this article.)

Seven hexagonal channels were filled with sand. A density of sand was between 1.41 and 1.54 g/cm^3, with an average density of 1.45 g/cm^3. The height of sand was from 74.5 cm to 78.1 cm (measured from the beginning of a fission column). The channels with sand were placed in the center of the reactor core. Twelve fuel assemblies with an average enrichment of 3.6% were placed around the channels with sand (see Figs. 2c and 3). Several critical experiments were performed, and the average moderator level is listed in Table 3. The experiment was also performed without insertion of sand and is also referred to as a void experiment.

2.2. Reaction rates measurement

Two sets of activation foils were used during irradiation with the 7 sand channels (Case 3). The first set, described in Table 1 and Fig. 4, was placed in a central tube of one fuel assembly. As can be seen in the table, the activation foils were placed in four axially different positions. The positions in Table 1 were measured from the beginning of the fission column. Due to the fact that the position 9 was near to the moderator level and due to the problems with MCNP calculation near to the moderator level (see Ref. [9]), the results from this position were not used in the evaluation.

The second set was placed into an aluminum capsule filled with sand, and the capsule was placed into the center of sand poured in the experimental channel. The center of the capsule was in the middle of the critical moderator level. The used activation foils are described in Table 2.

The Net Peak Areas (NPA) of irradiated activation foils were measured in the end cap position of HPGe detector with well-defined efficiency curve [10]. The measured NPA was used for determination of the reaction rates employing Eq. (1) and Eq. (2). The True Summation Correction Factor was applied for ^{198}Au, ^{182}Ta, ^{58}Co, ^{59}Fe, and ^{46}Sc measurement (see Refs. [11]).

$$A_{End.} = NPA(T_{Meas.}) \times \frac{\lambda}{\varepsilon \times \eta \times N} \times \frac{1}{(1 - e^{\lambda T_{Meas.}})} \times \frac{1}{e^{\lambda \Delta T}} \times k_{TSCF} \quad (1)$$

$$q = \frac{A_{End.}}{1 - e^{\lambda T_{Irr.}}} \quad (2)$$

Where:

- q - the reaction rate of activation during irradiation batch
- λ - the decay constant of the radioisotope considered

Table 1
Used activation detectors in fuel.

Position	Position [cm]	Foil	Reaction	Energy [keV]	Branching ratio
3	12.9	Ni	^{58}Ni(n,p)^{58}Co	810	0.9945
		Au	^{197}Au(n,g)^{198}Au	411	0.9562
5	22.9	Ni	^{58}Ni(n,p)^{58}Co	810	0.9945
		Au	^{197}Au(n,g)^{198}Au	411	0.9562
7	32.9	Ni	^{58}Ni(n,p)^{58}Co	810	0.9945
		Au	^{197}Au(n,g)^{198}Au	411	0.9562
9	42.9	Ni	^{58}Ni(n,p)^{58}Co	810	0.9945
		Au	^{197}Au(n,g)^{198}Au	411	0.9562

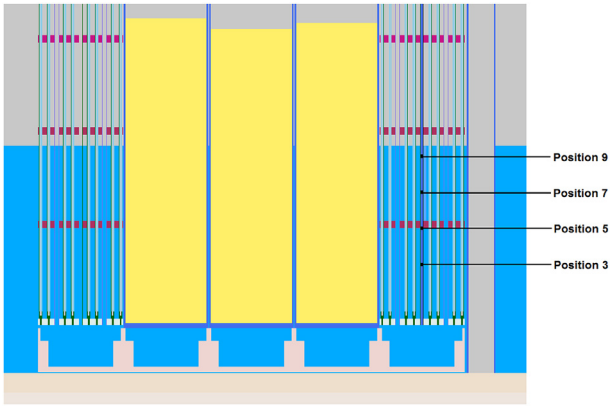

Fig. 4. Positions of activation detectors in fuel.

- $T_{meas.}$- a time of measurement by the HPGe
- ΔT - the time between the end of irradiation and the start of the HPGe measurement
- $NPA(T_{Meas.})$ - the Net Peak Area (the measured number of counts)
- ε - the gamma branching ratio
- η - the detector efficiency (determined via MCNP6 calculation)
- N - the number of target isotope nuclei
- K_{TSCF} – true summation correction factor
- $T_{Irr.}$- the end of the irradiation period

2.3. Calculations – MCNP

Criticality and neutron spectra for reaction rates determination

Table 2
Used activation detectors in capsule in sand.

Foil	Reaction	Energy [keV]	Branching ratio
Cu	$^{63}Cu(n,g)^{64}Cu$	511	0.3520
Au	$^{197}Au(n,g)^{198}Au$	411	0.9562
Ta	$^{181}Ta(n,g)^{182}Ta$	1121	0.3524
Ta	$^{181}Ta(n,g)^{182}Ta$	1221	0.2723
Ni	$^{58}Ni(n,p)^{58}Co$	810	0.9945
Fe	$^{54}Fe(n,p)^{54}Mn$	834	0.9998
Fe	$^{58}Fe(n,g)^{59}Fe$	1099	0.5650
Ti	$^{47}Ti(n,p)^{47}Sc$	159	0.6830

were calculated using MCNP6.2 [12] code. All materials excluding silicon and uranium were fixed in ENDF/B-VII.1 library [13] to suppress the other possible effects to criticality which are not being investigated in this study. In the case of criticality, uranium was defined from the ENDF/B-VII.1 or ENDF/B-VIII.0 [3] libraries. For reaction rate determination, uranium was taken from the ENDF/B-VII.1 library.

Silicon was defined from the ENDF/B-VII.1, ENDF/B-VIII.0 or from the new silicon INDEN [2] evaluations. Two TSL matrixes for SiO_2 were tested. TSL matrix from ENDF/B-VII.1 library was applied with silicon in the same library. ENDF/B-VIII.0 contains thermal data for different phases (α and β) of SiO_2, nevertheless, they differ from each other by temperature. Thus, the new TSL matrix for appropriate temperature (i.e. α-phase) was tested together with silicon in the same library and with the new silicon INDEN evaluation. Obtained results were compared with the results of the core without any insertion.

Criticality calculations were performed with 40,000 neutrons per generation and 5050 generations (5000 active and 50 inactive) and resulted in a standard deviation of 0.00005 k_{eff}. Spectra calculations for reaction rates determination were performed with 40,000 neutrons per generation and 1,000,050 generations (1,000,000 active and 50 inactive). The spectra were calculated in the 640 group structure, and the results were convoluted with the respective cross-sections. The IRDFF-II dosimetry cross-sections [14] were used for the reaction rates determination. The obtained reaction rates in the sand were normalized using the comparison of measured reaction rates in fuel with calculated reaction rates in fuel.

2.4. Calculations – SCALE

Sensitivity calculations were performed using SCALE6.2.3/TSUNAMI-3D code [15] with ENDF/B-VII.1 continuous energy cross-sections [13]. Detailed models of the cores were developed, and the Iterated Fission Probability method was applied [16]. Calculation of the case with crystalline silicon was performed with 50,000 neutrons per generation and 30,000 active generations, other sensitivity calculations were performed with 50,000 neutrons per generation and 15,000 active generations. This number of generations was necessary for sufficient sensitivity uncertainties. It was shown previously that the applied SCALE models agree well with the respective MCNP models [17,18].

3. Results and discussions

Experimentally determined critical levels of experiments with silicon together with the respective voided experiments are listed in Table 3. It is obvious that the insertion of sand into the center of the core decreases critical moderator level. This is caused by the moderation effects coming from silicon and oxygen (mostly due to the oxygen as can be found in Table 10). Opposite to that, the insertion of crystalline silicon has a negative effect on criticality, therefore the critical moderator level has increased. Nevertheless, the crystalline silicon influence was relatively small.

3.1. Comparison of calculations and experiments: criticality

The crystalline silicon results of the MCNP criticality calculations can be found in Table 4. In the case when the fuel is defined from the ENDF/B-VIII.0 the INDEN evaluation gives better results than the ENDF/B-VII.1 library (shown by the smaller difference between calculation with and without silicon). However, the crystalline silicon case features a relatively small amount of silicon and the difference between results is very close to the statistical uncertainty to make any conclusion.

The results of criticality calculations of the second experiment with small amount of sand (Case 2) are listed in Table 5. These results were obtained using various combinations of silicon cross-section. The calculation using the new INDEN evaluation and ENDF/B-VIII.0 together with the new TSL matrix gives the result closest to the void experiment. Opposite to that, the application of the old TSL matrix increases the bias between calculations of the case with and without sand. The results indicate that the main improvement was done in the TSL matrix because it caused a larger reduction of the discrepancy.

The third experiment featuring the largest amount of sand is listed in Table 6. As can be seen, the used computational model has

Table 3
Critical moderator levels in different LR-0 experiments.

	Case 1 Crystalline silicon	Case 2 One sand channel	Case 3 Seven sand channels
With insertion	56.907 ± 0.010 cm	48.833 ± 0.060 cm	45.726 ± 0.014 cm
Void experimental channel	56.260 ± 0.064 cm	55.722 ± 0.034 cm	57.468 ± 0.010 cm

Table 4
MCNP criticality calculations results of the experiment with the crystalline silicon insertion (Case 1).

Case 1 - Crystalline silicon			Case 1 - Void+Aluminum holder	
Silicon	Fuel	k_{eff}	Fuel	k_{eff}
INDEN	ENDF/B-VIII.0	1.00270	ENDF/B-VIII.0	1.00265
INDEN	ENDF/B-VII.1	1.00164	ENDF/B-VII.1	1.00146
ENDF/B-VII.1	ENDF/B-VIII.0	1.00288		
ENDF/B-VII.1	ENDF/B-VII.1	1.00175		
ENDF/B-VIII.0	ENDF/B-VIII.0	1.00291		
ENDF/B-VIII.0	ENDF/B-VII.1	1.00162		

Table 5
MCNP criticality calculations results of the experiment with the one sand channel (Case 2).

Case 2 - One sand channel			Case 2 - Void	
SiO_2	Fuel	k_{eff}	Fuel	k_{eff}
INDEN + TSL	ENDF/B-VIII.0	0.99938	ENDF/B-VIII.0	0.99958
INDEN + TSL	ENDF/B-VII.1	0.99885	ENDF/B-VII.1	0.99898
INDEN	ENDF/B-VIII.0	1.00049		
INDEN	ENDF/B-VII.1	0.99998		
ENDF/B-VIII.0 + TSL	ENDF/B-VIII.0	0.99975		
ENDF/B-VIII.0 + TSL	ENDF/B-VII.1	0.99920		
ENDF/B-VIII.0	ENDF/B-VIII.0	1.00089		
ENDF/B-VIII.0	ENDF/B-VII.1	1.00045		
ENDF/B-VII.1 + old TSL	ENDF/B-VIII.0	1.00104		
ENDF/B-VII.1 + old TSL	ENDF/B-VII.1	1.00061		
ENDF/B-VII.1	ENDF/B-VIII.0	1.00096		
ENDF/B-VII.1	ENDF/B-VII.1	1.00034		

Table 6
MCNP criticality calculations results of the experiment with seven sand channels (Case 3).

Case 3 - Seven sand channels			Case 3 - Void	
SiO_2	Fuel	k_{eff}	Fuel	k_{eff}
INDEN + TSL	ENDF/B-VIII.0	1.00318	ENDF/B-VIII.0	1.00340
INDEN + TSL	ENDF/B-VII.1	1.00234	ENDF/B-VII.1	1.00255
INDEN	ENDF/B-VIII.0	1.00503		
INDEN	ENDF/B-VII.1	1.00413		
ENDF/B-VIII.0 + TSL	ENDF/B-VIII.0	1.00377		
ENDF/B-VIII.0 + TSL	ENDF/B-VII.1	1.00288		
ENDF/B-VIII.0	ENDF/B-VIII.0	1.00576		
ENDF/B-VIII.0	ENDF/B-VII.1	1.00492		
ENDF/B-VII.1 + old TSL	ENDF/B-VIII.0	1.00608		
ENDF/B-VII.1 + old TSL	ENDF/B-VII.1	1.00530		
ENDF/B-VII.1	ENDF/B-VIII.0	1.00564		
ENDF/B-VII.1	ENDF/B-VII.1	1.00484		

a relatively large bias also in the void case. It is assumed that this is caused by the larger dimensions of the core. Larger dimensions and higher material content increase the influence of manufacturing and operational uncertainties. The main source of uncertainties is outer cladding diameter having influence about 80 pcm, the other main uncertainties are fuel assembly pitch and fuel enrichment. The total one sigma uncertainty is estimated to be around 100 pcm. The positive bias based on neglection of ^{234}U is about 247 pcm for small core and 139 pcm for bigger core. The assumed level of ^{234}U concentration is based on experimental data from Hungarian group. More details can be found in Ref. [8]. These uncertainties together with the limitation in the accuracy of nuclear data used in the calculation are assumed to be the main reason for discrepancies between calculation and experiment. Nevertheless, the comparison of the calculation with and without sand shows the larger improvement in the new INDEN evaluation and the TSL matrix. This is the same trend as in the previous case, and it is evident that the larger amount of sand highlights the influence of improvement of silicon cross-sections.

3.2. Comparison of calculations and experiments: reaction rates

The energy dependence of dosimetry cross sections used in the reaction rate determination is plotted in Fig. 5. An energy-dependent cumulative contribution to the reaction rate for every reaction is plotted in Fig. 6. Used dosimetry reactions cover a spectrum from thermal energies up to 20 MeV. Copper and ^{58}Fe activation detectors were used for the description of the thermal region. Gold and tantalum describe well the resonance part of spectrum, and other reactions are important for the fast part of spectrum.

The calculated reaction rates were compared to the

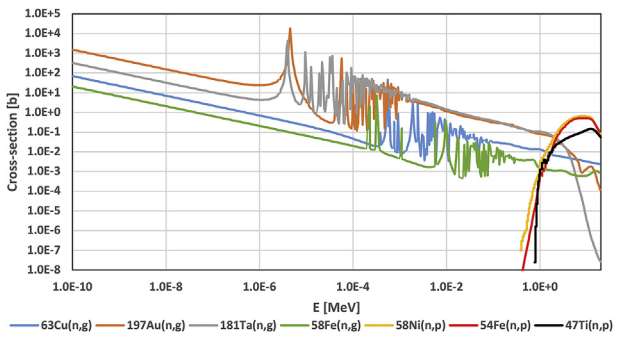

Fig. 5. Cross-sections used for reaction rates determination.

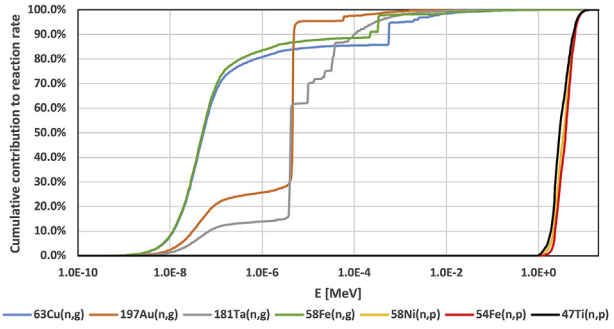

Fig. 6. Cumulative contribution of reaction rates.

Table 7
C/E-1 value of measured reaction rates in sand. Uranium cross section in the calculation was taken from the ENDF/B-VII.1 library.

Reaction	Mean [1/s] (INDEN)	Uncertainty	INDEN + TSL	INDEN without TSL	ENDF/B-VIII.0 + TSL	ENDF/B-VIII.0 without TSL	ENDF/B-VII.1 + old TSL	ENDF/B-VII.1 without TSL
^{197}Au(n,g)	5.680E-27	4.5%	−6.4%	−2.5%	−5.3%	−0.9%	4.0%	−1.1%
^{181}Ta(n,g)	2.039E-27	4.5%	−0.1%	2.3%	0.6%	3.9%	6.5%	3.4%
^{63}Cu(n,g)	7.764E-29	6.0%	−3.5%	9.5%	−0.8%	13.0%	10.5%	12.9%
^{58}Fe(n,g)	2.218E-29	4.8%	−3.8%	9.5%	−1.1%	13.1%	10.7%	13.0%
^{58}Ni(n,p)	8.209E-31	4.5%	4.0%	4.2%	4.3%	4.8%	4.6%	4.7%
^{47}Ti(n,p)	1.516E-31	4.5%	5.2%	5.4%	5.4%	6.0%	5.8%	6.0%
^{54}Fe(n,p)	5.606E-31	8.6%	5.6%	5.8%	5.9%	6.4%	6.1%	6.3%

Table 8
C/E-1 value of measured reaction rates in sand, both results normalized to calculation with TSL. Uranium cross section in the calculation was taken from the ENDF/B-VII.1 library.

Reaction	Mean [1/s]	INDEN + TSL	INDEN without TSL	difference
^{197}Au(n,g)	5.680E-27	−6.4%	−2.0%	−4.4%
^{181}Ta(n,g)	2.039E-27	−0.1%	2.9%	−3.0%
^{63}Cu(n,g)	7.764E-29	−3.5%	10.1%	−13.6%
^{58}Fe(n,g)	2.218E-29	−3.8%	10.1%	−13.9%
^{58}Ni(n,p)	8.209E-31	4.0%	4.8%	−0.7%
^{47}Ti(n,p)	1.516E-31	5.2%	6.0%	−0.8%
^{54}Fe(n,p)	5.606E-31	5.6%	6.3%	−0.7%

experimentally determined values. This comparison can be found in Table 7. This table contains data which were each normalized by fuel reaction rates calculation with the same library. The main sources of uncertainties in reaction rates are as follows: Statistical uncertainties of the scaling factor, measurement with HPGe detector, and reaction rate determination of several pieces of activation detectors. Another source of uncertainty is the uncertainty of efficiency calculation with the HPGe detector.

It is obvious that the satisfactory results were obtained by the calculation with the INDEN evaluation together with the new TSL matrix for sand. The application of ENDF/B-VIII.0 with the new TSL matrix gives satisfactory results too. The usage of ENDF/B-VII.1, no matter with or without TSL, gives results with large discrepancies. The results show that the calculation without the new TSL matrix gives unsatisfactory results for the ^{63}Cu(n,g) and ^{58}Fe(n,g) reactions. These reactions are very sensitive in the thermal region, therefore, the data indicates that the missing TSL matrix leads to bad description of neutron flux at thermal energies.

Table 8 presents results obtained with INDEN evaluation. Both groups of results are normalized by calculation with INDEN evaluation with the TSL matrix for sand. It is evident that the differences are especially in the ^{63}Cu(n,g) and ^{58}Fe(n,g) reactions. These results are consistent with the previous table.

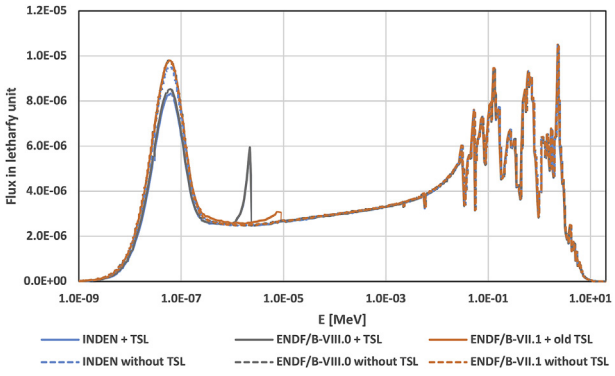

Fig. 7. Calculated spectra in the capsule with activation detectors in sand.

The results plotted in Fig. 7 are very surprising. The figure shows the neutron spectra calculated in the capsule with activation detectors. The compared results were obtained by calculations using different silicon evaluation with and without TSL matrix for sand. The application of the TSL matrix reduces the neutron flux in the energy ranges between 1.0E-8 and 1.0E-7 MeV. This is an expected fact because due to molecular effects, the collision rate is higher (due to lower energy transfer in elastic scattering) and the radiative capture does not change. The figure also shows unexpected and spurious peaks. The bigger one can be found in neutron spectra obtained using the new TSL matrix for sand. It is located in the region from 1 eV to 2.3 eV. The smaller one, located in the region from 3.5 ev to 9 eV, is visible in neutron spectrum obtained using old TSL matrix for sand.

Their occurrence is, however, clear from Fig. 8, where a significant gap is observed in the curve of the INDEN TSL matrix (yellow dashed line in Fig. 8) starting at 2.3 eV compared to the original total cross section data (blue dashed line) which are taken for the calculation from the fast energies until the energy of 2.3 eV. This abrupt depression in the cross-section causes the rise of the observed significant peak at 2.3 eV. At the same time, there comes substantial contribution to reaction rates of described monitors in the range of epithermal neutrons due to this peak. A similar issue can by found also in the curve for ENDF/B-VII.1 TSL matrix (red dashed line), but this curve continues approximately to 9 eV and the gap at this energy between TSL matrix and original cross-section is lower which implicates lower peak.

3.3. Results from sensitivity analyses

The main silicon sensitivities are listed in Table 9. These results were obtained by calculation in the TSUNAMI sequence. It can be seen that a radiative capture and an elastic scattering are the most important reactions. The radiative capture is the most important

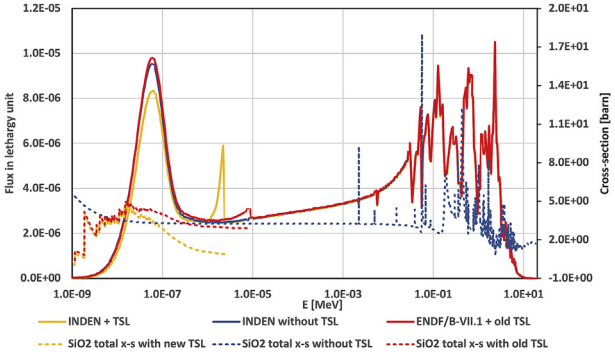

Fig. 8. Silicon dioxide total cross-section comparison with and without the application of TSL matrices together with corresponding neutron flux. (For interpretation of the references to color in this figure legend, the reader is referred to the Web version of this article.)

Table 9
Sensitivities of the main reactions in silicon.

Nuclide	Reaction	Sensitivity		
		Case 1 Crystalline Silicon	Case 2 One sand channel	Case 3 Seven sand channels
^{28}Si	n,g	−1.50E-3 ± 8.75E-7	−3.00E-3 ± 1.89E-6	−5.93E-3 ± 2.58E-6
^{28}Si	n,n	7.21E-4 ± 2.52E-5	3.49E-3 ± 4.65E-5	6.22E-3 ± 6.50E-5
^{28}Si	n,n'	2.43E-4 ± 3.37E-6	6.42E-4 ± 5.83E-6	9.21E-4 ± 7.38-E6
^{28}Si	total	−6.25E-4 ± 2.54E-5	1.01E-3 ± 4.70E-5	1.04E-3 ± 6.54E-5

Table 10
Comparison of total isotopic sensitivities in sand.

Nuclide	Case 2 One sand channel		Case 3 Seven sand channels	
	Sensitivity	Ratio	Sensitivity	Ratio
^{16}O	1.18E-02	90.6%	2.01E-02	93.9%
^{28}Si	1.01E-03	7.8%	1.04E-03	4.9%
^{29}Si	1.51E-04	1.2%	1.87E-04	0.9%
^{30}Si	6.63E-05	0.5%	7.13E-05	0.3%

reaction in crystalline silicon experiment. Opposite to that, the elastic scattering is the most important reaction in the sand.

The integrated sensitivities for nuclides in the sand are listed in Table 10. A comparison of Tables 9 and 10 shows that the sensitivities of individual reaction are higher in the big experiment (Case 3). Nevertheless, the increase of main reactions is similar, on that account, the integrated sensitivity of silicon nuclides remains almost the same. The ratio column in Table 10 shows the ratio of sensitivity of each nuclide divided by the total sensitivity of sand. It is obvious that the oxygen is dominant nuclide in the sand.

Fig. 9, Fig. 10 and Fig. 11 show the sensitivity per unit lethargy for ^{28}Si radiative capture and elastic scattering cross-sections over a full neutron energy range in all experiments. It is not surprising that the shape in the sand experiments is similar. The comparison of Fig. 9 with Figs. 10 and 11 shows the higher elastic scattering importance in higher energies in the sand. The shape of the radiative capture sensitivities is almost identical, the only difference is the absolute value of the sensitivities.Fig. 12 shows the shape of oxygen elastic scattering sensitivities in the sand. It can be seen that the shape is similar at high energies, and some differences in the shape are visible between 0.01 and 1 eV.

4. Conclusions

Experimental validation of newly evaluated silicon cross-

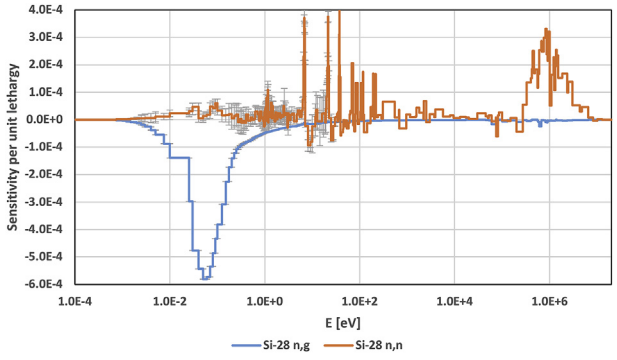

Fig. 9. Silicon radiative capture and elastic scattering sensitivities in crystalline silicon (Case 1). (For interpretation of the references to color in this figure legend, the reader is referred to the Web version of this article.)

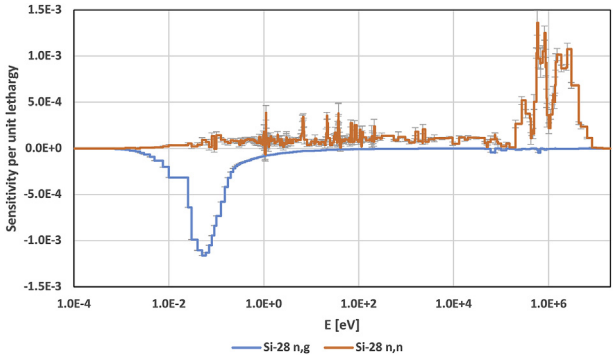

Fig. 10. Silicon radiative capture and elastic scattering sensitivities in the one sand channel (Case 3). (For interpretation of the references to color in this figure legend, the reader is referred to the Web version of this article.)

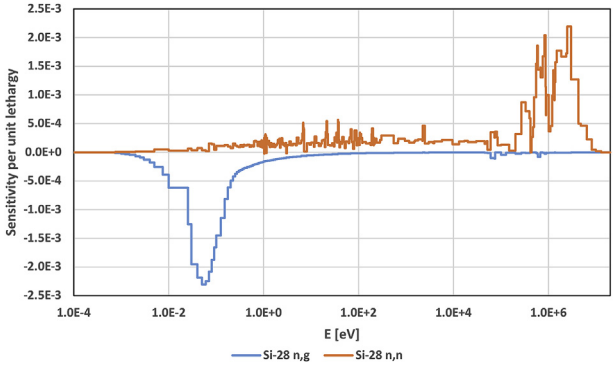

Fig. 11. Silicon radiative capture and elastic scattering sensitivities in seven sand channels (Case 3). (For interpretation of the references to color in this figure legend, the reader is referred to the Web version of this article.)

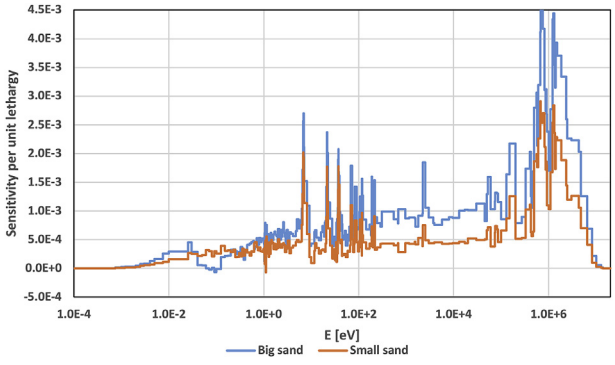

Fig. 12. Oxygen elastic scattering sensitivities in Case 2 and Case 3.

sections is an essential step following the new evaluation. The results show an improvement in the description of silicon cross sections with the new INDEN evaluation. Additionally, the new Thermal Scattering Matrix for sand in ENDF/B-VIII.0 is much better than the old version published in ENDF/B-VII.1. On the other hand, the neutron spectrum in the sand, calculated with the new TSL matrix, has unexpected peak around 1 eV, which however, has no clear, physical based explanation and is caused by the shifts in the cross-section data used for the calculation. This might be a problem in the new TSL matrix, and this matrix should be investigated in more detail. This validation was performed using the critical moderator level measurement together with the determination of reaction rates in silica sand.

Sensitivity study of the experiments, performed using the TSUNAMI/3D code, shows that from the point of view of neutronics oxygen is a dominant nuclide in the sand. The study also shows that the elastic scattering and the radiative capture are dominant reactions in silicon. The fact that the ^{28}Si is the dominant silicon nuclide in the sand is the expected fact because this isotope has two times higher nuclear density in sand and the silicon cross sections are relatively similar.

The last described experiment, consisting of 7 channels with sand, will be submitted as the ICSBEP benchmark.

Declaration of competing interest

The authors declare that they have no known competing financial interests or personal relationships that could have appeared to influence the work reported in this paper.

Acknowledgments

Presented results were obtained with the use of the infrastructure Reactors LVR-15 and LR-0, which is financially supported by the Ministry of Education, Youth and Sports - project LM2015074 and also financially supported by the Ministry of Education, Youth and Sports Czech Republic - project LQ1603 Research for SUSEN. This work has been realized within the SUSEN Project (established in the framework of the European Regional Development Fund in project CZ.1.05/2.1.00/03.0108 and of the European Structural Funds and Investment Funds (ESIF) in the project CZ.02.1.01/0.0/0.0/15_008/0000293), which is financially supported by the Ministry of Education, Youth and Sports - project LM2015093 Infrastructure SUSEN.

References

[1] R.L. Parker, Composition of the Earth's crust, U. S. Geol. Surv. Prof. Pap. 440-D (1967) 19, https://doi.org/10.3133/pp440D.
[2] M.T. Pigni, K.H. Guber, G. Arbanas, D. Wiarda, R. Capote, A. Trkov, Evaluation and validation of 28,29,30SI cross sections in the resolved resonance region, Oak Ridge, United States, https://doi.org/10.2172/1489565, 2019.
[3] D.A. Brown, M.B. Chadwick, R. Capote, A.C. Kahler, A. Trkov, M.W. Herman, A.A. Sonzogni, Y. Danon, A.D. Carlson, M. Dunn, D.L. Smith, G.M. Hale, G. Arbanas, R. Arcilla, C.R. Bates, B. Beck, B. Becker, F. Brown, R.J. Casperson, J. Conlin, D.E. Cullen, M.-A. Descalle, R. Firestone, T. Gaines, K.H. Guber, A.I. Hawari, J. Holmes, T.D. Johnson, T. Kawano, B.C. Kiedrowski, A.J. Koning, S. Kopecky, L. Leal, J.P. Lestone, C.R. Lubitz, J.I. Márquez Damián, C.M. Mattoon, E.A. McCutchan, S.F. Mughabghab, P. Navratil, D. Neudecker, G.P.A. Nobre, G. Noguere, M. Paris, M.T. Pigni, A.J. Plompen, B. Pritychenko, V.G. Pronyaev, D. Roubtsov, D. Rochman, P. Romano, P. Schillebeeckx, S. Simakov, M. Sin, I. Sirakov, B. Sleaford, V. Sobes, E.S. Soukhovitskii, I. Stetcu, P. Talou, I.J. Thompson, S.C. van der Marck, L. Welser-Sherrill, D. Wiarda, M.C. White, J.L. Wormald, R.Q. Wright, M.L. Zerkle, G. Žerovnik, Y. Zhu, ENDF/B-VIII.0: the 8th major release of the nuclear reaction data library with CIELO-project cross sections, new standards and thermal scattering data, Nucl. Data Sheets 148 (2018) 1–142, https://doi.org/10.1016/J.NDS.2018.02.001.
[4] A.Y. (Russian R.C. "Kurchatov I.) Gagarinski, Russian nuclear criticality experiments. Status and prospects, in: Proc. Int. Conf. Nucl. Energy New Eur. 2003, Nuclear Society of Slovenia, Slovenia, 2003, p. 10. https://inis.iaea.org/search/search.aspx?orig_q=RN:36115727. (Accessed 25 January 2019).
[5] O.N. Andrianova, G.B. Lomakov, G.N. Manturov, Examination of Silicon-28 and Uranium-235 resonance parameters based on integral and differential experiments, Nucl. Energy Technol. 2 (2016) 97–101, https://doi.org/10.1016/J.NUCET.2016.05.005.
[6] M. Košťál, J. Šoltés, L. Viererbl, Z. Matěj, F. Cvachovec, V. Rypar, E. Losa, Measurement of neutron spectra in a silicon filtered neutron beam using stilbene detectors at the LVR-15 research reactor, Appl. Radiat. Isot. 128 (2017) 41–48, https://doi.org/10.1016/J.APRADISO.2017.06.026.
[7] M. Košťál, V. Rypar, J. Milčák, V. Juříček, E. Losa, B. Forget, S. Harper, Study of graphite reactivity worth on well-defined cores assembled on LR-0 reactor, Ann. Nucl. Energy 87 (2016) 601–611, https://doi.org/10.1016/J.ANUCENE.2015.10.010.
[8] M. Košťál, V. Rypar, E. Losa, M. Schulc, E. Novák, B. Jánský, M. Veškrna, F. Mravec, Z. Matěj, F. Cvachovec, VVER-1000 Physics Experiments Hexagonal Lattices (1.275 Cm Pitch) of Low Enriched U(3.3 wt.% U235)O2 Fuel Assemblies in Light Water with Graphite and Fluoride Salt Insertions in Central Assembly, 2016.
[9] M. Košťál, M. Švadlenková, P. Baroň, V. Rypar, J. Milčák, Determining the axial power profile of partly flooded fuel in a compact core assembled in reactor LR-0, Ann. Nucl. Energy 90 (2016) 450–458, https://doi.org/10.1016/J.ANUCENE.2015.12.028.
[10] M. Košťál, M. Schulc, V. Rypar, E. Losa, N. Burianová, J. Šimon, M. Mareček, J. Uhlíř, Validation of zirconium isotopes (n,g) and (n,2n) cross sections in a comprehensive LR-0 reactor operative parameters set, Appl. Radiat. Isot. 128 (2017) 92–100, https://doi.org/10.1016/j.apradiso.2017.06.023.
[11] E. Tomarchio, S. Rizzo, Coincidence-summing correction equations in gamma-ray spectrometry with p-type HPGedetectors, Radiat. Phys. Chem. 80 (2011) 318–323, https://doi.org/10.1016/J.RADPHYSCHEM.2010.09.014.
[12] C.J. Werner, MCNP users manual-code version 6.2. https://laws.lanl.gov/vhosts/mcnp.lanl.gov/pdf_files/la-ur-17-29981.pdf, 2017.
[13] M.B. Chadwick, M. Herman, P. Obložinský, M.E. Dunn, Y. Danon, A.C. Kahler, D.L. Smith, B. Pritychenko, G. Arbanas, R. Arcilla, R. Brewer, D.A. Brown, R. Capote, A.D. Carlson, Y.S. Cho, H. Derrien, K. Guber, G.M. Hale, S. Hoblit, S. Holloway, T.D. Johnson, T. Kawano, B.C. Kiedrowski, H. Kim, S. Kunieda, N.M. Larson, L. Leal, J.P. Lestone, R.C. Little, E.A. McCutchan, R.E. MacFarlane, M. MacInnes, C.M. Mattoon, R.D. McKnight, S.F. Mughabghab, G.P.A. Nobre, G. Palmiotti, A. Palumbo, M.T. Pigni, V.G. Pronyaev, R.O. Sayer, A.A. Sonzogni, N.C. Summers, P. Talou, I.J. Thompson, A. Trkov, R.L. Vogt, S.C. van der Marck, A. Wallner, M.C. White, D. Wiarda, P.G. Young, ENDF/B-VII.1 nuclear data for science and technology: cross sections, covariances, fission product yields and decay data, Nucl. Data Sheets 112 (2011) 2887–2996, https://doi.org/10.1016/J.NDS.2011.11.002.
[14] A. Trkov, P.J. Griffin, S.P. Simakov, L.R. Greenwood, K.I. Zolotarev, R. Capote, D.L. Aldama, V. Chechev, C. Destouches, A.C. Kahler, C. Konno, M. Koštál, M. Majerle, E. Malambu, M. Ohta, V.G. Pronyaev, V. Radulović, S. Sato, M. Schulc, E. Šimečková, I. Vavtar, J. Wagemans, M. White, H. Yashima, IRDFF-II: a new neutron metrology library, Nucl. Data Sheets 163 (2020) 1–108, https://doi.org/10.1016/J.NDS.2019.12.001.
[15] B.T. Rearden, E.M.A. Jessee, SCALE Code System, 2017. ORNL/TM-2005/39.
[16] C.M. Perfetti, B.T. Rearden, W.R. Martin, SCALE continuous-energy eigenvalue sensitivity coefficient calculations, Nucl. Sci. Eng. 182 (2016) 332–353, https://doi.org/10.13182/NSE15-12.
[17] T. Czakoj, E. Losa, Criticality calculations and basic sensitivity/uncertainty investigation of LR-0 benchmark core, J. Nucl. Eng. Radiat. Sci. 5 (2019), 031401, https://doi.org/10.1115/1.4041692.
[18] T. Czakoj, E. Losa, M. Košťál, Design of a special core for large graphite insertion studies in the LR-0 reactor, in: PHYTRA4 – Fourth Int. Conf. Phys. Technol. React. Appl., Marrakech, Morocco, 2018, pp. 238–249.